Preparation of Gamma Poly-Glutamic Acid/Hydroxyapatite/Collagen Composite as the 3D-Printing Scaffold for Bone Tissue Engineering

Thu-Trang Nguyen
National Taipei University of Technology
Chih-Chien Hu
Chang Gung Memorial Hospital
Rajalakshmi Sakthivel
National Taipei University of Technology
Sasza Chyntara Nabilla
University of Oxford
Yu-Wen Huang
National Taipei University of Technology
Jiashing Yu
National Taiwan University
Nai-Chen Cheng
National Taiwan University Hospital
Yi-Jie Kuo
Taipei Medical University
Ren-Jei Chung (rjchung@ntut.edu.tw)
National Taipei University of Technology https://orcid.org/0000-0002-0655-3680

Research Article

Keywords: boneand osteochondral, 3D printing, collagen, polyglutamate acid, hydroxyapatite

Posted Date: February 18th, 2022

DOI: https://doi.org/10.21203/rs.3.rs-1306068/v1

Abstract

Background

Movement activities involving the role of articular cartilage and bones. The presence of cartilage enables bones to move over one another smoothly. However, repetitive microtrauma and ischemia as well as genetic effects can cause an osteochondral lesion. Numerous treatment methods such as microfracture, autograft, and allograft have been used, however, it possesses treatment challenges including extensive recovery time after surgery and financial burden on patients. Nowadays, tissue engineering approaches have been developed to repair bone and osteochondral defects using biomaterial implants to induce the regeneration of stem cells.

Methods

In this study, a collagen/γ-polyglutamate acid (PGA)/hydroxyapatite composite scaffold was fabricated using a 3D printing technique. A collagen/γ-PGA/hydroxyapatite 2D membrane was also fabricated for comparison. The scaffolds (4 layers) were designed with the size of 8 mm in diameter and 1.2 mm in thickness. The first layer was hydroxyapatite/γ-PGA and the second to fourth layers were collagen/γ-PGA. In addition, a 2D membrane was constructed from hydroxyapatite/γ-PGA and collagen/γ-PGA with a ratio of 1:3. The biocompatibility property and degradation activity were investigated for both scaffold and membrane samples. The rat bone marrow mesenchymal stem cells (*r*BMSCs) and human adipose stem cells (*h*ADSCs) were cultured on the samples and were tested *in-vitro* to evaluate cell attachment, proliferation, and differentiation. The *in-vivo* experiments were performed in the rat and nude mice models.

Results

Finally, the *in-vitro* and *in-vivo* results show that the developed scaffold is of well biodegradation and biocompatible properties; the Col-HA scaffold enhances the mechanical properties for osteochondrogenesis in both in-vitro and animal trials.

Conclusions

It would be a great biomaterial application for bone and osteochondral regeneration.

1. Introduction

The anatomical disruption of cartilage and underlying bone results in the osteochondral defect (OCD) [1] as the reasons include repetitive microtrauma, ischemia, and the issue of genetic expression [2]. This defect may lead to disability, pain during every movement of the joint, and gradual deformation of bone

articulation [3]. One of the essential textures will be heavy influenced is subchondral bone. Which is a very unique structure that includes huge of the blood vessels supporting for osteogenesis and maintains sufficient biomechanical support for the upper articular cartilage [4]. To date, microfracture, autologous implantation, autograft transfer, autograft transplantation, allograft transplantation, and bone tissue engineering are the main surgical treatment methods. However, the limited donor site morbidity, immune and inflammatory responses, as well as the risk of disease transmission are the huge drawbacks of autograft and allograft [5]. While tissue engineering is an ultimate method that is widely recognized for bone regeneration without depending on donor sources [6] thanks to transplantable scaffolds. An ideal scaffold for tissue engineering should possess excellent biocompatibility and induce osteogeneration from multipotent mesenchymal stem cells (MSCs) [7] by providing the extracellular matrix and mimicking the microenvironment. Evolving the conventional techniques, 3D printing has demonstrated its great potential in producing 3D-highly-porous functional scaffolds for biomedical applications. Extrusion printing is the most widely used type among 3D-bioprinting techniques with the direct-write printing feature [8] and encourages the creation of new biocompatibility ink such as the vicious-polymer hydrogel.

Type I collagen is the majority polymer distribution of connective tissue in the hard bone, skin, and blood vessels, which plays an important role in bone reconstruction [9] via RGD sequences that are the excellent specific bioligand for osteoblast adhesion with the interaction of α(2) β(1) integrins to stimulate bone morphogenetic protein [10]. Subchondral bone is a biphasic material. It comprises hydroxyapatite (HA) crystal inorganic section for stiffness, and an organic section of principally type I collagen, proteoglycan, glycosaminoglycans, and water affording elasticity and pliability [11] The bioactivity of HA is marked by osteoconductive and osteoinductive processes, that have been demonstrated for osseointegration supporting. The osteoinductive property of HA plays a guidance role for the formation of new bone on its surface down to the apertures of the implant body [12]. The HA osteoconductivity improves the attachment, proliferation, growth, and phenotype expression of the osteoblast in a direct contact way, hence a strong tissue-implant interface formation [13]. Owing to this property of HA stimulates tissue ingrowth that tolerates the bone neoformation even in the non-bone-forming zone. Besides, the HA coating for implanted improves initial mechanical stability post-implantation, which leads to a decrease in aseptic loosening. The HA aids the chemical bonding of the implanted tissue to native tissue with protein absorbable on the surface of the implant. Protein attendance on the surface is promising for an early healing outcome at the tissue-implant interface [14]. Unfortunately, HA disperses inhomogeneous and aggregation within the polymer matrix that results in nozzle clogging during printing and compromise of the mechanical scaffold [5]. However, γ-PGA possesses the excellent water absorption ability that can absorb moisture up to 1400–5000 times of its weight and encourage to be used as a wound-healing factor that is aimed for high levels of absorption of wound exudates [15]. Moreover, the L-isoform of γ-PGA has fascinated attention increasingly about biomedical applications because of its biodegradability and biocompatibility. Otherwise, this kind of polymer includes the negative charge [16, 17] that posses the largest affinity with the HA surface[18–20]. Therefore, γ-PGA is a great solution to dissolve HA for making the HA gel-like bioink structure.

The biodegradability and biocompatibility are the strengths of type I collagen for bone regeneration, the most drawback of their molecules own low mechanical properties. Fortunately, oligo proanthocyanidins (OPCs) are a good candidate for cross-linking to raise the mechanical properties of collagen scaffolds via oligomers of catechin and epicatechin and their gallic acid esters. Nimni *et al.* [21] reported that OPCs enhances collagen synthesis and increase the conversion speed of insoluble collagen from soluble collagen during development. Furthermore, OPCs possess numerous characteristics such as antioxidant, antiviral, antibacterial, anti-inflammatory, anticarcinogenic, vasodilatory actions, and anti-allergic. They can inhibit capillary hyperpermeability, platelet aggregation, and lipid peroxidation [22].

In this study, we aim to fabricate the 4-layer scaffold with two printheads bio-printer to mimic the articular cartilage structure and focus on simulate the function of subchondral bone with high molecular interaction of the first layer composed of HAp and γ-PGA equivalent subchondral bone layer, from the second layer to the fourth layer comprised type I collagen and γ-PGA that alike the superficial – middle – deep zone of articular cartilage. This scaffold is compared to collagen, collagen - γ-PGA scaffolds, and 2D membrane about the biocompatibility, biodegradation in the *in vitro* experiments then implanted into the rat and nude mice models. OPCs is used as biocompatible cross-linker for these scaffolds and membrane.

2. Materials And Methods

2.1. Materials

Type I collagen from bovine skin was purchased from Devro Pty Limited (Bathurst, Australia), Hydroxyapatite was acquired from Acros organic (Thermofisher Scientific, USA), γ-Polyglutamate was obtained from Vedan company (Taiwan), Oligo Proanthocyanins (OPCs) extracted from grape seed that was purchased from Gino Biotechnology Ltd. (Taipei, Taiwan).

2.2. Preparation of bioink for 3D printing

Hydroxyapatite and Gamma- Polyglutamate: First, 2g of γ-PGA completely dissolved into 10ml of deionized water, then added 6.5g hydroxyapatite powder (HA) into this solution and dissolved immediately until forming the slurry-gel-like structure.

Collagen and Gamma- Polyglutamate

Acetic acid was used as a solvent for both Collagen and γ-PGA. To avoid the poly-ion complex aggregation of collagen and γ-PGA. First, 20mg γ-PGA dissolved in 5ml deionized water by stirring to form a homogenous solution. Then added 450mg collagen powder, stirring vigorously to ensure that powder was uniformly distributed in the γ-PGA solution. Next, 5ml acetic acid was added to the solution. Since the collagen powder was already uniformly dispersed, the addition of acetic acid caused the dissolved immediately collagen powder, this procedure avoiding the aggregation due to the γ-PGA/collagen polyion complex. Thus, obtained a homogeneous solution.

Oligo Proanthocyanidin Solution

300 mg of oligo proanthocyanin was also dissolved into 30 ml of DI water to obtain a concentration of 10 mg/ml.

2.3. Fabrication of 3D scaffolds and 2-layer membrane of collagen/γ-polyglutamic acid/ hydroxyapatite

Composite scaffolds of collagen (Col), γ-polyglutamic acid (γ-PGA), hydroxyapatite (HA), and oligo proanthocyanidin (OPC) were fabricated by a 3D printing machine (Cellink, USA). There were three combinations of scaffolds composition such as: (I) the collagen with a concentration of 40 mg/ml [23] was then printed with a 30 mm length of 22G sterile needle (Cellink, USA), the pressure of 120 kPa, and speed of 4mm/s. (II) The collagen with a concentration of 45 mg/ml was mixed with 2 mg/ml γ-PGA were then printed with a 30 mm length of 22G needle, the pressure of 90 kPa, perimeter speed of 4mm/s, and infill speed of 3 mm/s. (III) The hydroxyapatite (650 mg/ml)/γ-PGA mixture (200 mg/ml) were printed as a first layer using 24 mm length of 22G needle, the pressure of 90 kPa, perimeter and infill speed of 4 mm/s and 3mm/s, respectively, thereafter the collagen (45 mg/ml)/γ-PGA (2 mg/ml) were also printed as second to fourth layers using 30 mm length of 22G needle, the pressure of 250 kPa, and speed of 3 mm/s to fabricate the scaffolds of collagen (45 mg/ml) combined with γ-PGA (2mg/ml) and hydroxyapatite (650 mg/ml) together with γ-PGA (200 mg/ml). The scaffolds were soaked in the OPC solution (10 mg/ml) for 4 hours to obtain crosslinking. The scaffolds were dried with freeze-drying for 24 hours. Figure 1 illustrates the concentration of fabricated 3D scaffolds and the arrangement of each layer. In addition, the two-layers membrane of collagen/γ-PGA/hydroxyapatite was also fabricated. The bottom layer consisted of a mixture of hydroxyapatite (650 mg/ml) and γ-PGA (200 mg/ml), then freeze-dried for 3 hours. The collagen (45 mg/ml) and γ-PGA (2 mg/ml) was applied as a second layer. A combination of all mixture was then soaked in OPC solution (10 mg/ml) for 4 hours and were dried with a freeze dryer for 24 hours.

2.4. Characterization of the scaffolds and membrane

2.4.1. Fourier-transform infrared spectroscopy (FT-IR)

FTIR analysis was performed to detect possible changes in the structure of collagen after oxidizing with γ-PGA and HA. Data were obtained on an FTIR spectrometer (Perkin Elmer, USA) with wavenumbers ranging from 4000 – 500 cm^{-1}.

2.4.2. X-Ray Diffraction

The XRD measurement is using the range of 20–60° in 2 thetas (θ) with CuKα (λ = 0.15405 nm) radiation as the source at a rate of 2° /min and with 1° glancing angle against the incident beam on the surface of the scaffold using the X-ray diffractometer (X'Pert3 Powder, PANalytical, Netherland) to detect the precipitation of apatite on the surface, which demonstrates the biological property of materials.

2.4.3. Field Emission Scanning electron microscope (FE-SEM)

The FE-SEM instrument (JEOL JSM-F100, USA) was used to observed the surface morphology of the scaffold and membrane. For SBF immersion, it was used to deposit the apatite appearance on the surface of scaffolds and membrane. The samples were gold-sputtered before observation. The surface of samples was captured at different magnifications, ranging from 25x, 85x, and 100x.

2.4.4. Compressive mechanical property

The mechanical properties were performed by Dynamic Mechanical Analyzer Q800 (TA Instrument, USA). The scaffolds specimens (Ø 8 x 2.5 mm) and membrane with dimensions of 8 × 8 × 2 mm (length × width × height) were loaded under ramp force from 0.2000 N/min to 18.0000 N of the Clamp Compression depend on Air Bearing Gas at 37℃. The uniaxial compressive force was applied to the hydrogel constructs until the point of failure. The compressive modulus was is then determined by the slope of the stress – strain curve. Each sample was measured at least in triplicate.

2.4.5 Rheological properties of hydrogels

The Col, Col-P, HA-P hydrogels were measured with a Modular Compact Rheometer (MCR 302, Anton Paar, Austria) to evaluate viscosity, storage modulus, and loss modulus under the cone CP25-1 for 8.2 minutes at room temperature. The complex viscosity and modulus changes over shearing frequency are recorded with Start Rheoplus software (Version 3.62, Anton Paar GmbH, Graz, Austria).

2.5. Degradation test, pore size, and porosity measurement

The degradation rates of the scaffold samples were studied by performing a degradation test. The scaffolds were soaked in 50 ml PBS at 37˚C on different days to evaluate the degradation activity. The weights of the scaffolds before and after soaking were used to calculate the percentage of degradation.

$$Degradationrate(\%) = \frac{W_w - W_0}{W_0} x100\%$$

1

where W_w is the weight after soaking and W_0 is the original height.

The pore size and connector size were measured by ImageJ software. The porosity was calculated according to the formula:

$$Porosity(\%) = \frac{W_{wet} - W_{dry}}{V_2 - V_3} x100\%$$

2

Where W_{wet} is the materials' weight after soaking with ethanol for quick sorption, Wdry is the free-dried materials' weight, V2 is the volume of solvent after soaking materials, and V3 is the volume of ethanol after the samples are taken out.

2.6. Surface deposition of calcium phosphate apatite

The solution was prepared by dissolving NaCl, $NaHCO_3$, KCl, K_2HPO_4, $MgCl_2.6H_2O$, $CaCl_2$, and Na_2SO4 in Tris-HCL buffer at pH 7.38 (37˚C). A bone-like apatite layer was allowed to nucleate and grow on the surface of the samples. After the completion of the 7, 14, and 21 days of incubation, the samples were taken out and freeze-dried. The apatite morphology was investigated with FE-SEM, and elemental composition was analyzed using the XRD. Prior to FE-SEM, the samples were coated with a platinum layer.

2.7. *r*BMSCs and *h*ADSCs for cell culture

*r*BMSCs were isolated from the bone marrow of Sprague Dawley (5 weeks old) rats. The bone marrow cells were flushed from SD rat femurs and tibias with Dulbecco's Modified Eagle's Medium (DMEM - Gibco, USA), supplemented with 10% FBS, 1% penicillin-streptomycin, 1% glutamine, and 1% non-essential amino acid. Cells were plated in a 75 cm^2 flask and incubated at 37℃ with 5% CO_2. After 4h, non-adherent cells and supernatant were removed. Thereafter, *r*BMSCs were purified and the medium was replaced every 72h. Passage 3–6 of *r*BMSCs were used for all experiments.

*h*ADSC were obtained from the National Taiwan University Hospital [24] was cultured in Dulbecco's Modified Eagle's Medium- F12 (DMEM - Gibco, USA), supplemented with 10% FBS, 1% penicillin-streptomycin, 1% glutamine, and 1% non-essential amino acid. Cells were cultured at 37℃ under 5% CO2, and the medium was renewed every two days until confluence was reached.

2.8. Cytotoxicity Test

Cell counting kit – 8 includes WST – 8 (2-(2-methoxy-4-nitrophenyl)-3-(4-nitrophenyl)-5-(2,4-disulfophenyl)-2H-tetrazolium, monosodium salt). This compound will produce a water-soluble formazan dye due to bioreduction when the presence of an electron carrier, 1-Methoxy PMS. Cellular dehydrogenases reduce WST-8 to an orange formazan product that is solubilized in the culture medium. The amount of formazan produced is directly proportional to the number of living cells. Since the CCK-8 solution is very stable and has little cytotoxicity. Cell Counting Kit-8 allows sensitive colorimetric assays for the determination of the number of viable cells in the proliferation assay. Therefore, we using the CKK-8 kit to count the quality of *r*BMSC and *h*ADSC viability that is seeded with the membrane and scaffolds.

On the first day, sterilizing the scaffolds and membrane under UV light for 30 minutes then put it in the 48-well plate with 200 µl medium in each well for their water absorption. The next day, aspirate all the old medium, then add 5 x 10^4 *r*BMSC, *h*ADSC, and 1 ml medium to each well, incubate for 1, 3, 7 days. Then replaced medium with 100 µl and 10 µl CKK-8 solution to each well, incubated at 37℃, 5% CO2 for 4

hours under protected light conditions. Transferred 100 µl supernatant to a new 96-well plate to absorb at 450 nm wavelength.

2.9. Fluorescence staining (DAPI)

DAPI is a fluorescence stain - photostability that label DNA and allow easy visualization of the nucleus in interphase cells and chromosome in mitotic cells. DAPI can associates with the minor groove of double-stranded DNA, with a preference for the adenine- thymine cluster via the permeable cell membrane. That is using to label nuclear DNA of cell growth when seed *h*ADSC with the scaffolds and membrane.

After 3 days incubation of 5 x 10^3/ml cell, aspirate medium from each well, washing with PBS solution 3 times, then put the scaffolds and membrane in the new 48-well plate. Next, add 500 µl DAPI reagent to each well in the light-protected condition, incubated within 15 minutes. Reaction finished, the scaffolds and membrane washing with PBS solution 3 times, cut the scaffold with the long dimension. Observed the fluorescence cell inside of composites under fluorescence microscopy.

2.10. Gene expression

*r*BMSCs have capable of differentiation to specific tissue depends on gene activities. Especially, when seeding *r*BMSC with the direct biomaterials that can stimulate the specific target gene expression. Here, we evaluate the Collagen type I (F: TCCAAGGAAATGGCAACTCAGCTC; R: GAAACAGACGGGGCCAACC), Collagen type 2 (F: TCGCTGGTGCTGCTGACGCTGCTCG, R: CTGAGGGCCAGGAGGTCCTCTGG), Aggrecan (F: GGCCATGGTCCTTCTATGAC, R: TGTTGACGAACTCCTGTTCC), and BMP-2 (F: TGCACCAAGATGAACACAGC, R: GTGCCACGATCCAGTCATTC) genes of *r*BMSC expression that compared to the house of keeping gene GAPDH (F: GTGAAGCTCATTTCCTGGTATG, R: AACTGAGGGCCTCTCTCTTG) when it is seeding with scaffolds and membrane.

After 14 days incubation of *r*BMSCs at a density of 5 x 10^4 *r*BMSC, harvest cell and extract mRNA with RNaesy Mini Kit (Qiagen, Germany), measure RNA with 10mM Tris-Cl, pH 7.5 for mRNA purification. cDNA synthesis by RevertAid First Strand cDNA Synthesis Kit (Thermo Scientific, USA). Finally, RT-PCR runs with Taqman™ Universal PCR Master Mix (Thermo Scientific, USA), PCR thermos cycle in the Applied Biosystems StepOnePlus ™ Real-Time PCR System includes step 1: 95°C for 10 min, 95 °C for 15s, 60°C for 1 min (40 cycles) and step 2: 25°C ∞. the results were analyzed by $2^{-\Delta\Delta Ct}$ method – where ΔΔCT= (C_T,target–$C_{T,GAPDH}$) experimental sample—($C_{T,target}$–$C_{T,\ GAPDH}$) control sample.

2.11 Quantitative immunoassay

The 5x10^4 of *h*ADSCs were seeded on the scaffolds and the membranes at 2, 5, and 7 days. The medium was switched to a serum-free medium for 24 hours. The supernatant was tested with bone morphogenetic protein 2 (BMP-2) Quantikine ELISA Kit (R&D system, USA) to evaluate the BMP-2 concentration.

2.12 In vivo experiment with nude mice and rat models and histological morphology

The biomaterials are assumed to direct differentiation BMSC. To demonstrate this hypothesis, biomaterial should be implanted into the animal model and observed histologically using staining techniques. Sprague Dawley® (SD) rats (5 weeks old) were used for *in vivo* experiments. The SD rats were acclimatized for at least one week before the experiment. The experiments were carried out in Chang Gung Memorial Hospital with their guidelines to care for and use animals. All the experiments were approved by Affiliated Institutional Animal Care and Use Committee (IACUC) under affidavit no. 2019102401. Diet was ad libitum rat chow and continuously supplied with water. To observe histological of *r*BMSC and *h*ADSC when implanted with the Col, Col-P, Col-HA scaffolds, and Col-HA-M membrane. The materials were seeded with 5 x 10^4 *r*BMSC for 7 days. Following that, transplanted directly the scaffold and membrane to the subcutaneous part of the back with 4 defects of the 15 Sprague Dawley® rats divide into 3 groups with different cages, group I includes 1 control rat, 3 material implanted rats, sacrificed after 1 week, group II similar to the previous but sacrificed after 2 weeks, and group III includes 7 rats with 1 controls rat and 6 rats carrying materials, then sacrificed after 4 weeks observed. Harvest the scaffold and membrane from the rat model after 1, 2, 4 weeks then sending to Taipei Pathology Institute to observed histological via H&E staining.

The experiment with the nude mice model is similar, however, mice carry 2 scaffolds/ membrane. A total of 21 mice were investigated that were divided into 3 groups, each group includes 1 control mice and 6 material implanted mice, sacrificed after 1, 2, and 4 weeks, respectively. Then the samples also using H&E staining to observed histology.

2.13 Statistical analysis

In this study, the data are represented as mean ± standard deviation. Student t-test two-tail was used for statistical analyses. p values < 0.05 were considered statistically significant. Origin 2019b software was used to evaluate FTIR, XRD, mechanical properties, and rheological results. The pore size, fluorescence, and histological image were measured and edited by ImageJ.

3. Results

3.1 Characterization of the 2D membrane and 3D scaffolds

Figure 2A shows the FT-IR spectrum of the three different scaffolds such as Col, Col-P, and Col-HA, and the membrane of Col-HA-M was immersed into the OPCs cross-linker. It can be seen that the type I collagen with OPCs shows the peaks at 3381 cm^{-1}, 1790 cm^{-1}, 1623 cm^{-1}, 1486 cm^{-1}, 1104 cm^{-1}, 913 cm^{-1} assigned to the N-H stretching, C-O stretching, C = C stretching, C-H bending, C-O stretching, and -C-H bending, respectively. All the Col peaks were regenerated and also the new peak arose at 1563 cm^{-1} (N-H

bending) signifying present in the scaffold of Col-P. Besides the scaffold of Col-HA shows the Col peaks with one weak intense peak at 1182 cm^{-1} (C-N stretching) and two strong intense peaks at 1032 cm^{-1} (C-O stretching) and 561 cm^{-1} (PO_4^{3-}) which is attributed to the HA presence in the Col-HA scaffold. Finally, the Col-HA membrane shows weak intense peaks. Due to the random arrangement of the Col-HA membrane.

Figure 2B-D present the surface morphology of scaffolds and membrane. In this study, the suitable pore size of our scaffolds is about 266 ± 5.87 μm (Figure 2D), the width of the connectors is 492 ± 3.36 μm (all of the scaffolds using the same needle size).

The rheological properties of hydrogels were evaluated, the frequency was set at the range of 0 to 20 Hz for storage modulus and loss modulus testing (Fig. 3A-B). The minimum storage modulus of collagen hydrogel was approximately 270 Pa, while that figure of collagen – γPGA hydrogel was around 187 Pa. The possible reason is due to poly-electrolyte interaction between collagen [25] and γPGA which reduce the viscosity of each other. For the Hydroxyapatite – γPGA hydrogel, the significantly higher minimum storage modulus value at around 18.4 kPa because of the much higher concentration of γPGA, which is consistent with higher pneumatic pressure of HA-P hydrogel in 3D printing.

Figure 3C-D indicated the compression mechanical properties of the scaffolds and membrane that were conducted at 37°C to mimic the bio-environment. The failure point of 3D scaffolds is much higher than that of the membrane. The threshold point of the membrane is at approximately 22.7 kPa while the Col and Col-P scaffold were failed at around 49.3 kPa and 36.46 kPa, respectively. The highest compressive stress was applied to the Col-HA scaffold is at about 111.09 kPa (Fig. 3C). Similarly, the compressive modulus of the specimens is reliable, the compressive Young's modulus of Col-HA scaffold possesses the highest at 272 kPa. It was increased 3 times compared to Col and Col-P group (102 and 97.8 kPa) and almost 5 times related to the Col-HA-M membrane (at 62.1 kPa). Overall, the results suggest that the Col-HA 3D scaffold has pretty good mechanical properties for bone regeneration and we used these materials for the following experiments.

3.2. Biocompatibility of the scaffolds and 2D membrane

The biomineralization of scaffolds in simulated body fluid (SBF) medium has become one of the most useful critical surface techniques to predict the in vivo bone bioactivity of a material [26] by the deposition of apatite minerals, consequently increasing biocompatibility. Figure 4 shows the surface of Col, Col-P, and Col-HA scaffolds and Col-HA-M membrane. On day 7, the apatite formation in the Col-P and Col-HA scaffolds is higher compared to the Col surface due to the similar structure of Collagen-γPGA. The increase in the soaking time is attributed to more apatite precipitation on the surface. After 21 days, the empty region of the scaffolds is filled with apatite. It indicates that the scaffolds showing good biocompatibility. In terms of biocompatibility, all samples are suitable to be used for biomedical applications due to high apatite absorption. XRD pattern was performed for further confirmation (Fig. 5). According to the JCPDS card No. 09-0432, it is found that the main diffraction peaks at 31.8, 45.5, and 56.5 degrees 2θ could be indexed to (211), (222), and (322) [27–29] planes matched the standard

hydroxyapatite diffraction peaks. It indicates that the surface scaffolds are composed of apatite deposition.

3.3 Biodegradability of collagen/γ-PGA/hydroxyapatite

Figure 6A shows the degradation behavior of the scaffolds as a function of time until equilibrium. The weight decreased gradually when immersing samples in PBS. The degradation rates of Col, Col-P and Col-HA scaffolds were 92.0 ± 1.5%, 92.2 ± 0.9%, 90.77 ± 0.4%, respectively, highest and reaches up to 76.6 ± 2.9% compared with the other scaffolds (76.6 ± 2.9% for Col and 81.9 ± 1.1%. for Col-P). The scaffolds were broken after 9 weeks of immersion. The degradation rate of the 2D Col-HA-M membrane is lower compared to 3D scaffolds. After 3 weeks, the degradation rate is 75.9 ± 3.6%. The equilibrium degradation rate is reached up to 36.06 ± 3.13%.

3.4 Cell viability and cell proliferation

The viability of *r*BMSC cells that were cultured in 3D scaffolds and the 2D membrane was evaluated by the CKK-8 kit. The numbers of living cells were expressed as OD values. The number of living cells increased when seeded with the composition of both 3D scaffolds and 2D membrane (Fig. 6B), indicating higher cell proliferation. Col-HA scaffold shows the OD value of 1.80 ± 0.32 compared to other scaffolds such as 0.95 ± 0.08 and 0.94 ± 0.20 for Col and Col-P, respectively. According to Zhang *et al.* 2020 [30], the collagen/hyaluronic acid gel used for cartilage generation was showed an OD value of 1.1 after 7 days of observation. In addition, Du *et al.* (2019) [6] reported that mesoporous bioactive glass (MBG)/polycaprolactone (PCL) scaffold used for human bone marrow stem cells (*h*BMSCs) proliferation study demonstrated the OD value of 1.5. In this study, Col-HA scaffolds present higher OD values which are proven as the microenvironment for the cells proliferated. The analogous results when seeding *h*ADSCs with our materials (Fig. 6C). The OD values of the Col-HA scaffold are highest (0.7126 ± 0.0025) compared to other scaffolds (~ 0.15–0.51). Figure 6D demonstrates DAPI staining results of the *h*ADSCs cultured on the Col, Col-P, Col-HA scaffolds as well as Col-HA-M membrane. The density of nuclei and cytoskeleton development are more highly developed on the Col-HA scaffold.

3.5 Gene Expression Analysis and quantitative ELISA assay

The genes expression such as type I and type II collagens, Aggrecan, and BMP-2 were examined. As shown in Fig. 7, the majority of these genes are upregulated to different degrees in the *r*BMSCs cells cultured in 3D collagen-based scaffolds, compared with those cultured on the 2D membrane, following culture for 14 days. The expression levels of type I collagen and BMP-2 in the Col-HA scaffold are upregulated and are directed to osteogenic. The type II collagen and Aggrecan were markedly upregulated in the Col-P scaffold which corresponds to chondrogenic for *r*BMCSs. Therefore, the scaffold with HA composition promotes the osteogenic, and γ-PGA tends to induce the chondrogenesis.

Figure 8 demonstrates the amount of BMP-2 in the different groups. The Col-HA scaffold exhibits an immense initial in the expression of the BMP-2 concentration after 2 days cultured. As the time increased, the expression of BMP-2 is significantly decreased on day 5 and then gradually increase on day 7 (Fig. 8).

Compared with those in the corresponding 2D membrane, the BMP-2 expression in the 3D form is higher such as follows the order of 817.17 ± 7.48 pg/ml, 556.25 ± 7.48 pg/ml, and 350.60 ± 7.477 pg/ml for Col, Col-P, and Col-HA-M, respectively. In general, all the 3D scaffolds and membrane possess biocompatibility and biodegradability, however, the Col-HA scaffold indicates the most suitable properties for *in-vitro* bone regeneration in this study.

3.6 *In vivo* biological evaluation

The histology of the scaffolds and membrane which were implanted subcutaneously in the nude mice and rat models are presented in Fig. 9 and Fig. 10, respectively. The color for both 3D scaffolds and 2D membrane does not change (brown color), therefore the barrier of seeded cells and native cells from the animal model could be recognized (blue arrow). After 4 weeks of implant, the Col-HA scaffold is filled with the cells (the purple color indicates the nuclei) and extracellular matrix (pink color). The cell density expanded on the Col-HA scaffold is the highest compared to other scaffold compositions and even new blood vessel information (the yellow arrow), which exhibit the osteogenesis character of subchondral bone because the osteocytes require vascular supply. However, the collagen with γ-polyglutamic acid shows more cell viability compared to pure collagen scaffold. In the Col-HA-M, the cells appear in an opposite way such as the cell core appearing on the surface of the membrane and the extracellular (ECM) matrix being inside.

4. Discussion

This study was designed to develop a multilayer scaffold that serves an osteochondral defect. The osteochondral is constructed of the subchondral bone plate and trabecular bone containing water and ECM. Their ECM is composed of organic matrix and inorganic hydroxyapatite which influence elasticity and material stiffness, respectively in the tissue [31]. One of the most vital roles of the subchondral is highly vascularized to facilitate the enrollment of progenitor cells. Thus, it has an extraordinary inherent potential for spontaneous remodeling and regeneration. Moreover, the subchondral bone is a complex interface between bone and cartilage, which is the key challenge for OCD repair and regeneration. As such, in the current research, we are looking for a multilayer 3D printing scaffold that possesses improved mechanical properties, biocompatibility, osteogenesis, and chondrogenesis properties.

From the bone tissue engineering point of view, the porosity of 3D printing scaffolds not only provides space for cell settlement and growth but also ensures the transport of nutrients and metabolites[7]. Generally, high porosities (> 80%) are evaluated as optimal for new bone tissue regeneration (Fig. 2B), and macroporosity with pore sizes in the range of 100–300 μm is beneficial to waste removal and nutrient supplement [32]. Because the size of osteoblasts is on the order of 10–50 μm, therefore, it prefers a larger pore for regenerating mineralized bone after implantation [33]. Besides, small pores favor hypoxic conditions and induce osteochondral formation before osteogenesis occurs, by contrast, larger pore scaffolds rapidly become well-vascularized and lead to direct osteogenesis [34]. Moreover, the rheological property of bio-ink gel is a decisive factor for the porosities of scaffold. Based on the concentration-dependent viscosity [35] of γPGA, a high amount of γPGA was applied to reduce the inhomogeneous

dispersion of hydroxyapatite in printing. Obviously, all the loss modulus of hydrogels were smaller than the storage modulus (G” < G’) that possess the suitable gel character for 3D direct-write extrusion printing[36] (Fig. 3A).

The fundamental character of 3D scaffold is machanical properties, our materials possess a significantly higher young modulus compared to Wong *et al.*'s (2017) report with the young modulus of the articular collagen type II construct was 9.86 KPa [37]. The young modulus property of scaffold is very important for bone tissue engineering due to reconstruction and load-bearing function at the same time. The Col-HA group shows the increasing load-bearing character thanks to the addition of hydroxyapatite in this composite and the alignment of materials in 3D shape with high exposure in cross-linker due to their porosity. While the Col-HA-M membrane has hydroxyapatite in its structure, the compressive modulus is still low because of the 2D structure that gets the lower density of cross-linker to become a better load-bearing candidate. Even compared to Col and Col-P scaffold, the compression stress of the 2D membrane is lower, this demonstrates the 3D scaffolds’ porosity is a central factor to induce their mechanical properties.

Initially of biocompatibility testing, after immersion in SBF, the apatite is formed in the Col, Col-P, and Col-HA scaffolds as well as the Col-HA-M membrane. However, the Col-HA-M scaffold shows a greatly reduced amount of apatite after 14 and 21 days of immersion as the decreased intensity peak (Fig. 5) due to decomposition. Which is the consequence of the less cross-linking between the high density of polymer compounds in the 2D membrane. Obviously, the lower molecular density leads to higher cross-linker formation in the 3D scaffolds. Otherwise, the apatite layer supports osteogenesis due to the formation of the tight chemical bond between osteocytes and materials [26]. Thus the 3D scaffolds present a better possibility for biocompatibility in general.

Due to the low mechanical properties of collagen, the OPC crosslinker was introduced in the system to maintain the mechanical stability of the biomaterials. If the degradation rate is too high, there is not enough mechanical strength to support the osteocytes/ chondrocytes formation. However, if the degradation is too low it could not create enough space for cell growth. Our biocompatible materials are stronger compare to the CS/HAp of the Nguyen *et al.* group, which is decomposed up to 46.37% after 28 days immersion in PBS [38]. The degradation rate of Col-HA and Col-HA-M is higher due to the greater released rate of hydroxyapatite. It can be explained as the interaction between collagen and hydroxyapatite is the self-organization of the HAp directional deposition on collagen and surface interaction in the composite. The direction between HAp and collagen is restricted by a covalent bond between COO^- and Ca^{2+} to maintain regular coordination [39]. Once this bonding is disturbed, the hydroxyapatite will be released. It is totally different to neither multi-bonding between collagen and γ-PGA with polyelectrolyte complexes that consisted of collagen as a polyelectrolyte cationic and γ-PGA as the polyelectrolyte anionic [25]; nor multiple hydrogen bonds are formed between OPC (-OH) and Collagen (-HO and -N2H) [40].

Then the cell viability was influenced by the mechanical and chemical characters of the scaffolds. It could be explained by hydroxyapatite of Col-HA enhances the mechanical properties of the scaffold that can induce significant growth of cell lines [41]. Although the Col-HA-M membrane group indicates the pretty good results of cell viability, the Col-HA group presents the greater cell proliferation since the ideal macropore size of 3D scaffold plays the role to mimic the microenvironment for both rat mesenchymal stem cells and human adipose stem cells growth. The osteogenesis and chondrogenesis of Col-P and Col-HA were evaluated by gene expression for further information. As mentioned by Yang *et al.* (2020), the Ca^{2+} ion released from hydroxyapatite expedites osteoconductive and osteoinductive processes via FAK-ERK pathway activation [5]. In addition, Ca^{2+} and L-arginine work together to express the coupling pathway of NO/cGMP in osteogenesis and angiogenesis[42, 43]. Bone morphogenetic protein (BMP-2) is a potent osteogenic factor that promotes differentiation of mesenchymal stem cells into fibroblast and chondroblasts [44] Moreover, BMP-2 and BMP-4 divert aortic calcifying vascular cells to osteogenic fates [45] [46]. The amount of BMP-2 specifies the character of materials in differentiation stem cells for both initial and later phases, especially in the Col-HA group.

In the animal trials, we use the rat model to mimic the clinic microenvironment that provides humidity, relevant nutrients, gaseous concentrations, and growth factors [47], for which purposes of cytotoxicity testing. While the nude mice's lack of thymus results in T-cell deficiency and immunodeficient, thereby being able to accept the foreign tissue [48, 49] and the formation of blood vessels appears from the second week. It demonstrates our materials are greatly biocompatible for both the normal immune system and immunodeficient. Even though the ectopic subcutaneous implant is the least invasive model, it could be use used for primary screening of MSCs from different tissue sources and new scaffold materials [49, 50]. Besides, the blood vessels formation is a great supporting for spontaneous regeneration. There is potential healthy crosstalk between the subchondral bone and the articular cartilage that leads to coupled bone remodelling in order to preserve homeostasis and repair microdamage [51].

Despite the fact that the collagen-hydroxyapatite-gamma glutamate scaffold demonstrated great mechanical properties, biocompatibility, and upregulation of osteochondrogenesis, we still lack a clear understanding of how these materials affect the immune system and metabolism in a specific way. Also, our future research will be carried out on site-specific implants to gain a better understanding of load-bearing and biocompatible characteristics in the in-situ regeneration of bone and osteochondral tissues.

5. Conclusion

This study focused on the preparation of Col/HAp/γ-PGA composite using a 3D printing technique to fabricate 8mm x 8mm x 1.2 mm multilayer scaffolds. It is possible to print a multilayer scaffold with the first layer of hydroxyapatite and γ-PGA mixture, the 2nd – 4th layer of collagen-γ-PGA solution using 2 print heads of a 3D direct-write bio-printer. The scaffold has good biodegradation with the weight loss reach up to 26%. Thanks to the 3D structure and OPC crosslinker, the mechanical properties of the Col-HA scaffold increase 5 times compared to the 2D membrane. The biomaterial scaffold and membrane

showed good biocompatibility at FE-SEM and XRD results when immersing in the stimulate body fluid, along with CCK-8 assay. The result of genes specific differentiation shows that the Col, Col-HA scaffolds direct *r*BMSC with the tendency growing to bone regeneration, by contrast, Col-P improves the growth of the cell for cartilage restoration. The Col-HA possesses the potential of osteogenic via stimulated BMP-2 expression and encouraged *h*ADSCs proliferation and differentiation. This study developed a feasible way to fabricate the multilayer scaffold that combines ceramic and polymer matrix for bone regeneration and potential osteochondral regeneration.

Abbreviations

γ-PGA: γ-polyglutamate acid

3D: three dimensions

2D: two dimensions

*r*BMSCs: rat bone mesenchymal stem cells

*h*ADSCs: human adipo stem cells

OCD: osteochondral defect

HA: hydroxyapatite

OPCs: Oligo Proanthocyanidins

FT-IR: Fourier-transform infrared spectroscopy

XRD: X-Ray Diffraction

FE-SEM: Field Emission Scanning electron microscope

MCR: Modular Compact Rheometer

PBS: Phosphate Buffer Saline

FBS: Fetal Bovine Serum

SBF: Simulated Body Fluid

SD: Sprague Dawley

DMEM: Dulbecco's Modified Eagle's Medium

BMP-2: bone morphogenetic protein 2

IACUC: Affiliated Institutional Animal Care and Use Committee

H&E: Hemoxylin and Eosin

CCK-8: Cell counting kit - 8

Declarations

Ethics approval and consent to participate

Procedures involving animals were approved by the Ethics Committee of the Taipei Medical University and Chang Gung Memorial University. All the experiments were approved by Affiliated Institutional Animal Care and Use Committee (IACUC) under affidavit no. 2019102401.

Consent for publication

Not applicable.

Availability of data and materials

The datasets used and/or analyzed during the current study are available from the corresponding authors on reasonable request.

Competing interests

The authors declare that they have no known competing financial interests or personal relationships that could have appeared to influence the work reported in this paper.

Funding

This research was supported financially by the Ministry of Science and Technology of Taiwan (MOST 107-2221-E-027-014; MOST 109-2622-E-027-003-CC3), National Taipei University of Technology and Chang Gung Memorial Hospital Joint Research Program (NTUT-CGMH-110-03 (CORPG3L0121))

Authors' contributions

CCH, YJK and RJC were responsible for the conception, methodology, supervision and funding acquisition of this research. TTN, RS, SCN and YWH were responsible for the investigation, methodology, formal analysis, data curation and validation of this study. JY and NCC provided resources. TTN drafted the manuscript. CCH, RS, SCN, JY, YJK and RJC revised the manuscript. All the authors read and approved the final manuscript.

References

1. Planell JA: **Bone repair biomaterials**: Elsevier; 2009.

2. Durur-Subasi I, Durur-Karakaya A, Yildirim OSJTEjom: **Osteochondral lesions of major joints**. 2015, **47**(2):138.
3. Medvedeva EV, Grebenik EA, Gornostaeva SN, Telpuhov VI, Lychagin AV, Timashev PS, Chagin ASJIjoms: **Repair of damaged articular cartilage: current approaches and future directions**. 2018, **19**(8):2366.
4. Zhou L, Gjvm VO, Malda J, Stoddart MJ, Lai Y, Richards RG, Ki-wai Ho K, Qin LJAHM: **Innovative Tissue-Engineered Strategies for Osteochondral Defect Repair and Regeneration: Current Progress and Challenges**. 2020, **9**(23):2001008.
5. Yang Y, Zhang Q, Xu T, Zhang H, Zhang M, Lu L, Hao Y, Fuh JH, Zhao XJB: **Photocrosslinkable nanocomposite ink for printing strong, biodegradable and bioactive bone graft**. 2020, **263**:120378.
6. Du X, Wei D, Huang L, Zhu M, Zhang Y, Zhu YJMS, C E: **3D printing of mesoporous bioactive glass/silk fibroin composite scaffolds for bone tissue engineering**. 2019, **103**:109731.
7. Chen X, Fan H, Deng X, Wu L, Yi T, Gu L, Zhou C, Fan Y, Zhang XJN: **Scaffold structural microenvironmental cues to guide tissue regeneration in bone tissue applications**. 2018, **8**(11):960.
8. Comeau P, Willett TJMS, C E: **Triethyleneglycol dimethacrylate addition improves the 3D-printability and construct properties of a GelMA-nHA composite system towards tissue engineering applications**. 2020, **112**:110937.
9. Chung R-J, Wang A-N, Wang H-Y, Wu Y-CJJotACS: **Investigation of collagen/tricalcium silicate/carboxymethyl cellulose composite bone glue for drug controlled release**. 2017, **53**(2):329-342.
10. Santin M: **Strategies in regenerative medicine**: Springer; 2009.
11. Stewart HL, Kawcak CEJFivs: **The importance of subchondral bone in the pathophysiology of osteoarthritis**. 2018, **5**:178.
12. Kowal TJ, Hahn NC, Eider S, Marzillier JY, Fodera DM, Thamma U, Jain H, Falk MMJBM: **New bioactive glass scaffolds with exceptional qualities for bone tissue regeneration: response of osteoblasts and osteoclasts**. 2018, **13**(2):025005.
13. Fu D-l, Jiang Q-h, He F-m, Yang G-l, Liu LJJoZUSB: **Fluorescence microscopic analysis of bone osseointegration of strontium-substituted hydroxyapatite implants**. 2012, **13**(5):364-371.
14. Habibah TU, Salisbury HG: **Hydroxyapatite dental material**. In: *StatPearls [Internet].* StatPearls Publishing; 2019.
15. Liu W-C, Wang H-Y, Lee T-H, Chung R-JJMS, C E: **Gamma-poly glutamate/gelatin composite hydrogels crosslinked by proanthocyanidins for wound healing**. 2019, **101**:630-639.
16. Ogunleye A, Bhat A, Irorere VU, Hill D, Williams C, Radecka IJM: **Poly-γ-glutamic acid: production, properties and applications**. 2015, **161**(1):1-17.
17. Shih I, Van Y, Yeh L, Lin H, Chang YJBt: **Production of a biopolymer flocculant from Bacillus licheniformis and its flocculation properties**. 2001, **78**(3):267-272.

18. Koutsopoulos S, Dalas EJL: **Hydroxyapatite crystallization in the presence of amino acids with uncharged polar side groups: glycine, cysteine, cystine, and glutamine**. 2001, **17**(4):1074-1079.
19. Koutsopoulos S, Dalas EJJoc, science i: **The crystallization of hydroxyapatite in the presence of lysine**. 2000, **231**(2):207-212.
20. Comeau P, Willett TJSr: **Impact of side chain polarity on non-stoichiometric nano-hydroxyapatite surface functionalization with amino acids**. 2018, **8**(1):1-11.
21. Han B, Jaurequi J, Tang BW, Nimni MEJJoBMRPAAOJoTSfB, The Japanese Society for Biomaterials,, Biomaterials TASf, Biomaterials tKSf: **Proanthocyanidin: a natural crosslinking reagent for stabilizing collagen matrices**. 2003, **65**(1):118-124.
22. Fine AMJAmrajoct: **Oligomeric proanthocyanidin complexes: history, structure, and phytopharmaceutical applications**. 2000, **5**(2):144.
23. Lee C-F, Hsu Y-H, Lin Y-C, Nguyen T-T, Chen H-W, Nabilla SC, Hou S-Y, Chang F-C, Chung R-J: **3D Printing of Collagen/Oligomeric Proanthocyanidin/Oxidized Hyaluronic Acid Composite Scaffolds for Articular Cartilage Repair**. 2021, **13**(18):3123.
24. Wu K-H, Mei C, Lin C-W, Yang K-C, Yu JJJoMCB: **The influence of bubble size on chondrogenic differentiation of adipose-derived stem cells in gelatin microbubble scaffolds**. 2018, **6**(1):125-132.
25. Tsao CT, Chang CH, Lin YY, Wu MF, Han JL, Hsieh KHJJob, polymers c: **Tissue response to chitosan/γ-PGA polyelectrolyte complex using a rat model**. 2011, **26**(2):191-206.
26. Kokubo T, Takadama HJB: **How useful is SBF in predicting in vivo bone bioactivity?** 2006, **27**(15):2907-2915.
27. An L, Li W, Xu Y, Zeng D, Cheng Y, Wang GJCI: **Controlled additive-free hydrothermal synthesis and characterization of uniform hydroxyapatite nanobelts**. 2016, **42**(2):3104-3112.
28. Wei K, Kim B-S, Kim I-SJM: **Fabrication and biocompatibility of electrospun silk biocomposites**. 2011, **1**(4):275-298.
29. Hui D, Goodridge RD, Scotchford C, Grant DMJAM: **Laser sintering of nano-hydroxyapatite coated polyamide 12 powders**. 2018, **22**:560-570.
30. Zhang Y, Cao Y, Zhao H, Zhang L, Ni T, Liu Y, An Z, Liu M, Pei RJJoMCB: **An injectable BMSC-laden enzyme-catalyzed crosslinking collagen-hyaluronic acid hydrogel for cartilage repair and regeneration**. 2020, **8**(19):4237-4244.
31. Madry H, van Dijk CN, Mueller-Gerbl MJKs, sports traumatology, arthroscopy: **The basic science of the subchondral bone**. 2010, **18**(4):419-433.
32. Wu C, Ramaswamy Y, Zreiqat HJAb: **Porous diopside (CaMgSi2O6) scaffold: a promising bioactive material for bone tissue engineering**. 2010, **6**(6):2237-2245.
33. Abbasi N, Hamlet S, Love RM, Nguyen N-TJJoSAM, Devices: **Porous scaffolds for bone regeneration**. 2020, **5**(1):1-9.
34. Hutmacher DW, Schantz JT, Lam CXF, Tan KC, Lim TCJJote, medicine r: **State of the art and future directions of scaffold-based bone engineering from a biomaterials perspective**. 2007, **1**(4):245-260.

35. Ho GH, Ho TI, Hsieh KH, Su YC, Lin PY, Yang J, Yang KH, Yang SCJJotCCS: **γ-polyglutamic acid produced by Bacillus Subtilis (Natto): Structural characteristics, chemical properties and biological functionalities**. 2006, **53**(6):1363-1384.
36. Shin YJ, Shafranek RT, Tsui JH, Walcott J, Nelson A, Kim D-HJAB: **3D bioprinting of mechanically tuned bioinks derived from cardiac decellularized extracellular matrix**. 2021, **119**:75-88.
37. Wong C-C, Chen C-H, Chiu L-H, Tsuang Y-H, Bai M-Y, Chung R-J, Lin Y-H, Hsieh F-J, Chen Y-T, Yang T-LJTAjosm: **Facilitating in vivo articular cartilage repair by tissue-engineered cartilage grafts produced from auricular chondrocytes**. 2018, **46**(3):713-727.
38. Nga NK, Tam LTT, Ha NT, Viet PH, Huy TQJRA: **Enhanced biomineralization and protein adsorption capacity of 3D chitosan/hydroxyapatite biomimetic scaffolds applied for bone-tissue engineering**. 2020, **10**(70):43045-43057.
39. Kikuchi M, Ikoma T, Itoh S, Matsumoto HN, Koyama Y, Takakuda K, Shinomiya K, Tanaka JJCS, Technology: **Biomimetic synthesis of bone-like nanocomposites using the self-organization mechanism of hydroxyapatite and collagen**. 2004, **64**(6):819-825.
40. Mao H, Chen C, Liao X, Shi BJJoMCAC: **Catalytic hydrogenation of quinoline over recyclable palladium nanoparticles supported on tannin grafted collagen fibers**. 2011, **341**(1-2):51-56.
41. Chen X, Bai S, Li B, Liu H, Wu G, Liu S, Zhao YJIjon: **Fabrication of gelatin methacrylate/nanohydroxyapatite microgel arrays for periodontal tissue regeneration**. 2016, **11**:4707.
42. Yang Y, Xu T, Zhang Q, Piao Y, Bei HP, Zhao XJS: **Biomimetic, Stiff, and Adhesive Periosteum with Osteogenic–Angiogenic Coupling Effect for Bone Regeneration**. 2021, **17**(14):2006598.
43. Coletta C, Papapetropoulos A, Erdelyi K, Olah G, Módis K, Panopoulos P, Asimakopoulou A, Gerö D, Sharina I, Martin EJPotNAoS: **Hydrogen sulfide and nitric oxide are mutually dependent in the regulation of angiogenesis and endothelium-dependent vasorelaxation**. 2012, **109**(23):9161-9166.
44. Gary F, Budd R, Gabriel S: **Kelley's Textbook of Rheumatology, Chapter 102 "Proliferative Bone Diseases,"**. In.: Philadelphia, PA: Saunders; 2012.
45. Wang M, Monticone RE, Lakatta EG: **The Aging Arterial Wall**. In: *Handbook of the Biology of Aging.* Elsevier; 2016: 359-389.
46. Shao J-S, Cai J, Towler DAJA, thrombosis,, biology v: **Molecular mechanisms of vascular calcification: lessons learned from the aorta**. 2006, **26**(7):1423-1430.
47. Horner EA, Kirkham J, Wood D, Curran S, Smith M, Thomson B, Yang XBJTEPBR: **Long bone defect models for tissue engineering applications: criteria for choice**. 2010, **16**(2):263-271.
48. Hoffman RMJP-DMMoC: **In Memoriam: Jørgen Rygaard (1934–2016), Father of Patient-Derived Mouse Models of Cancer and Modern Cancer Research**. 2017:1-6.
49. Giannoudis P, Jones E, Yang X, McGonagle D: **Mesenchymal stem cells and skeletal regeneration**: Academic Press; 2013.

50. El-Gendy R, Yang XB, Newby PJ, Boccaccini AR, Kirkham JJTEPA: **Osteogenic differentiation of human dental pulp stromal cells on 45S5 Bioglass® based scaffolds in vitro and in vivo**. 2013, **19**(5-6):707-715.
51. Findlay DM, Kuliwaba JSJBr: **Bone–cartilage crosstalk: a conversation for understanding osteoarthritis**. 2016, **4**(1):1-12.

Figures

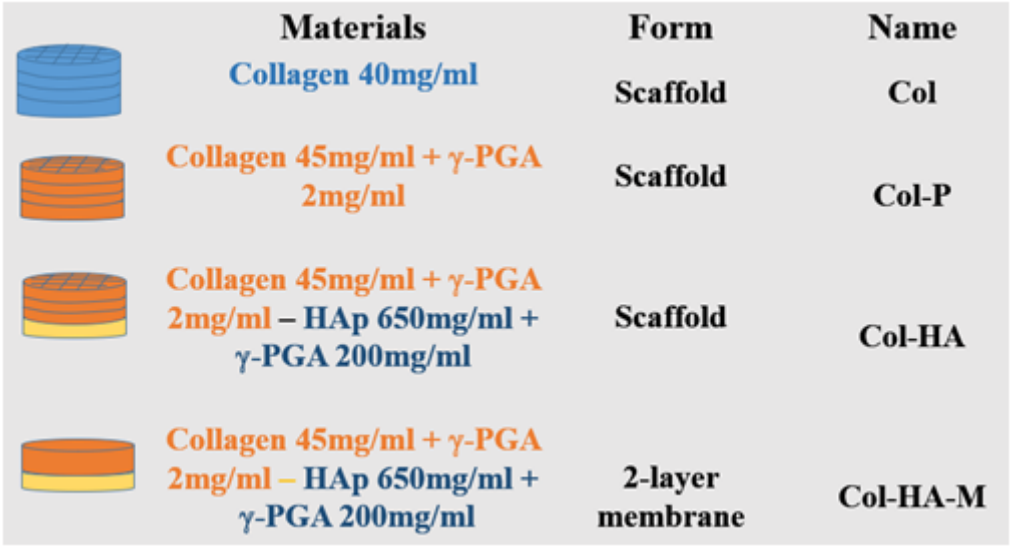

Figure 1

Fabrication of 3D scaffolds and 2-layer membrane with different composition and concentration

Figure 2

(A)FTIR spectra of collagen, collagen/g-PGA, collagen/g-PGA/hydroxyapatite 3D scaffolds, and 2D membrane- top view and underneath. **(B)**The porosity of materials. **(C)**The surface topography of scaffolds and membrane **(D)** Pore size and connector size measurement (n=5).

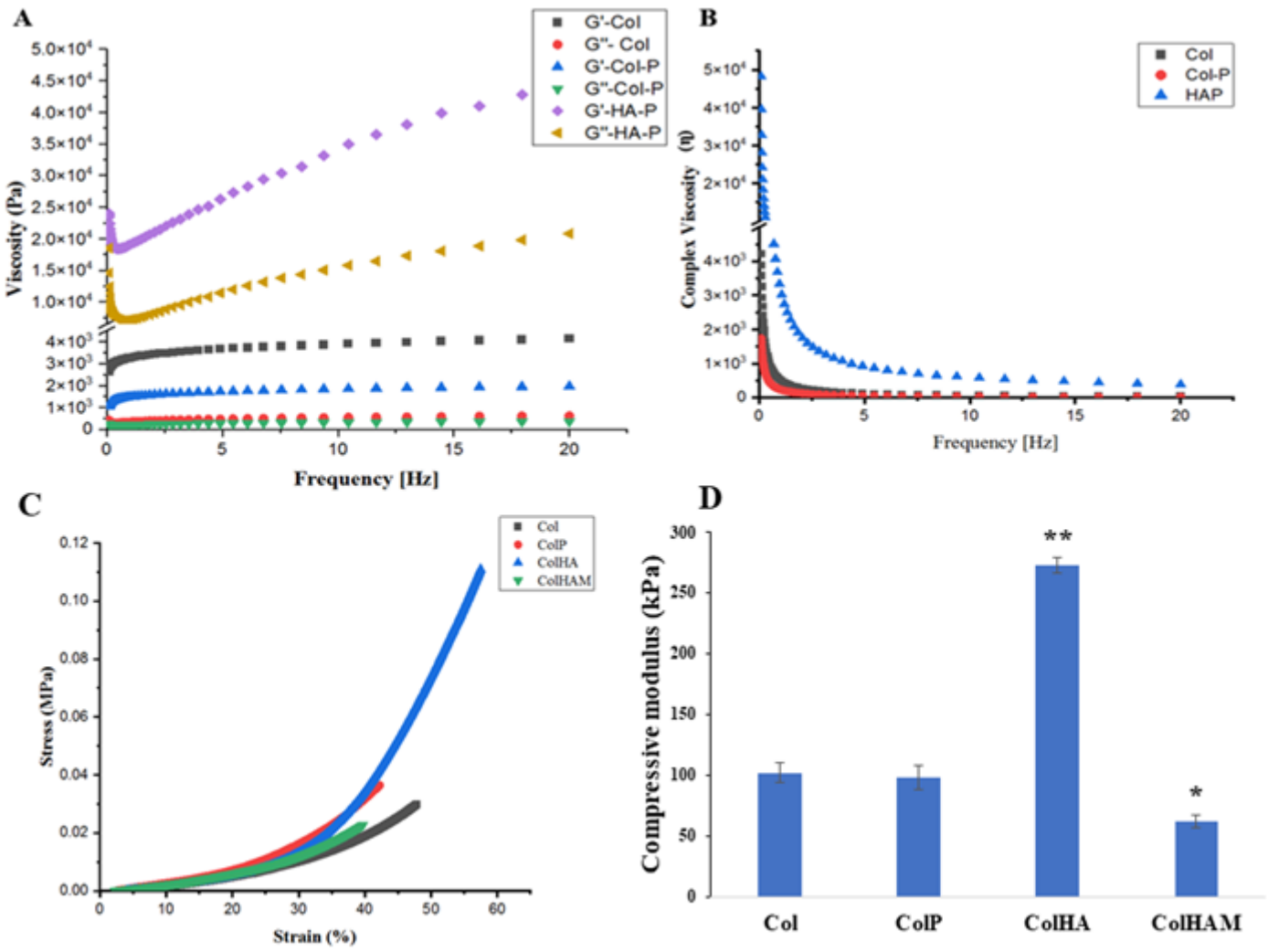

Figure 3

Rheological behavior of Col, Col-P, HA-P hydrogel. A. Storage modulus (G') and loss modulus (G"). B. Complex viscosity (η). Mechanical property of Col-HA membrane. C. Compression testing stress-strain curve of scaffolds and membrane. D. Compressive young's modulus from the slope of the stress-strain curve (n = 3, * $p < 0.05$, ** $p < 0.01$).

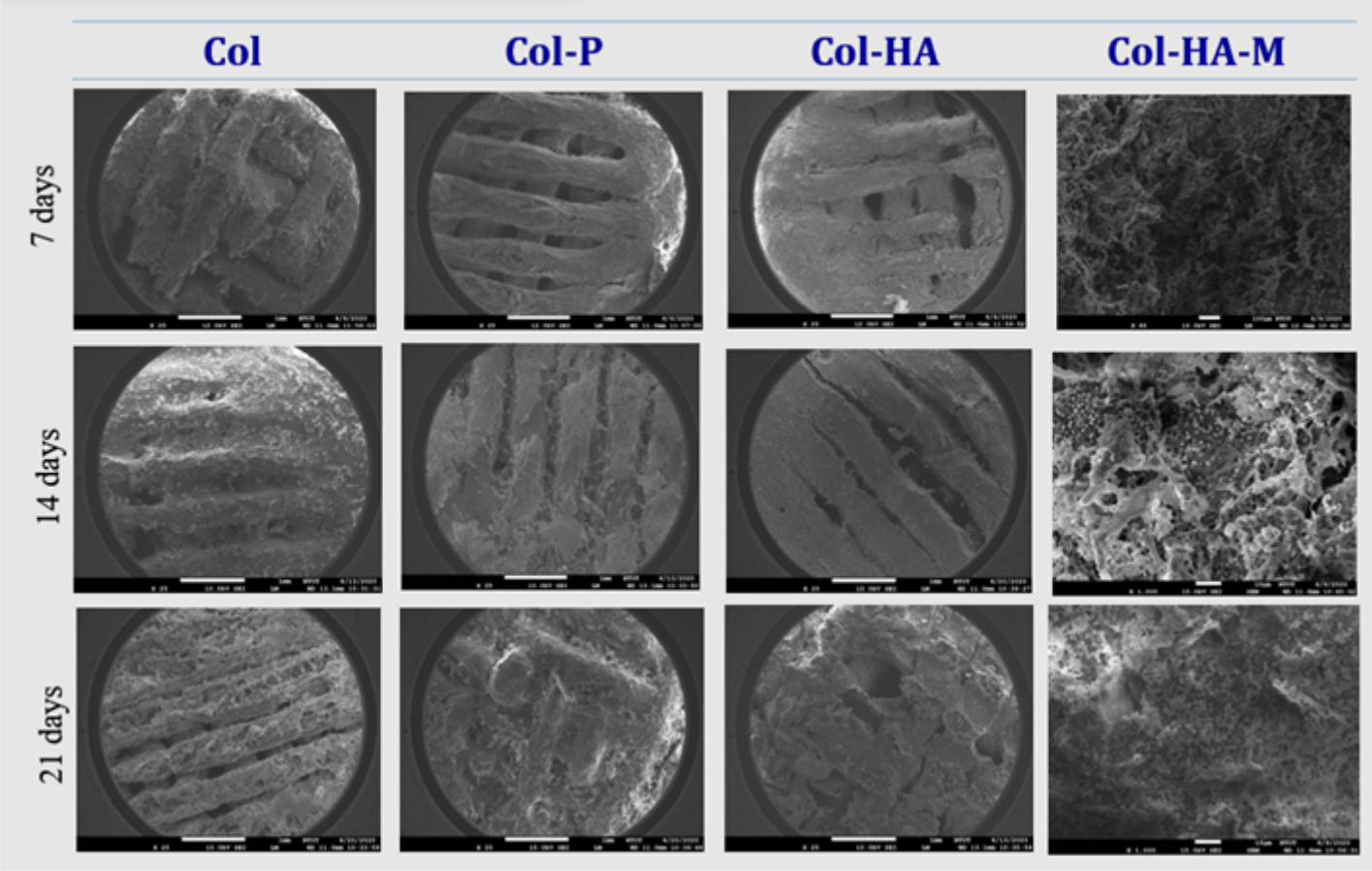

Figure 4

Apatite layers formation on the surface of 3D scaffolds (Col, Col-P, Col-HA) and 2D membrane (Col-HA-M) after immersion in the simulated body fluid for 7, 14, and 21 days (the scale bar of 1mm and 100μm for the scaffold and membrane, respectively).

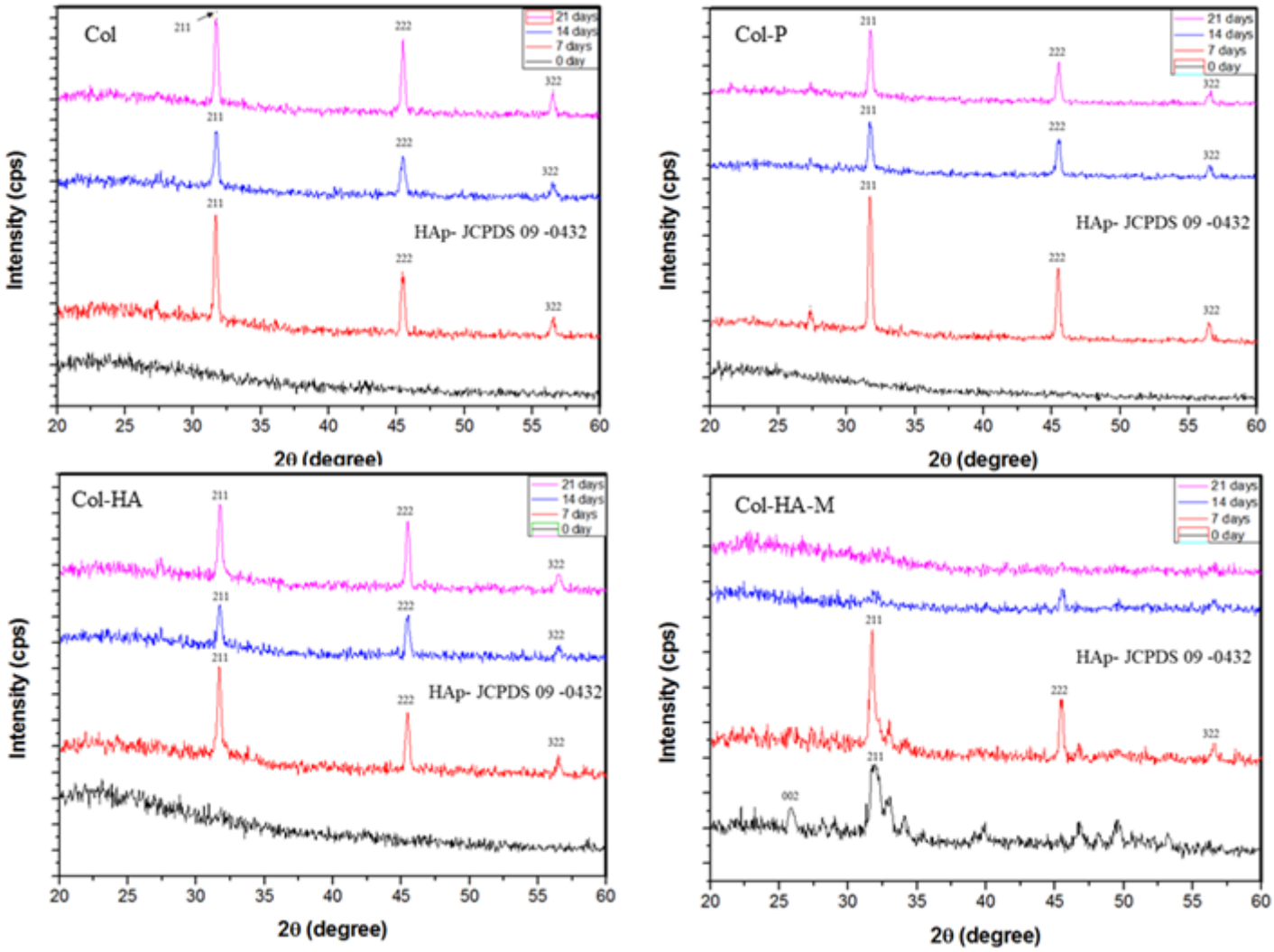

Figure 5

XRD patterns of the 3D scaffolds (Col, Col-P, Col-HA) and 2D membrane (Col-HA-M) with peaks of appetite crystal structure as a function of FBSimmersion time on 7, 14, and 21 days.

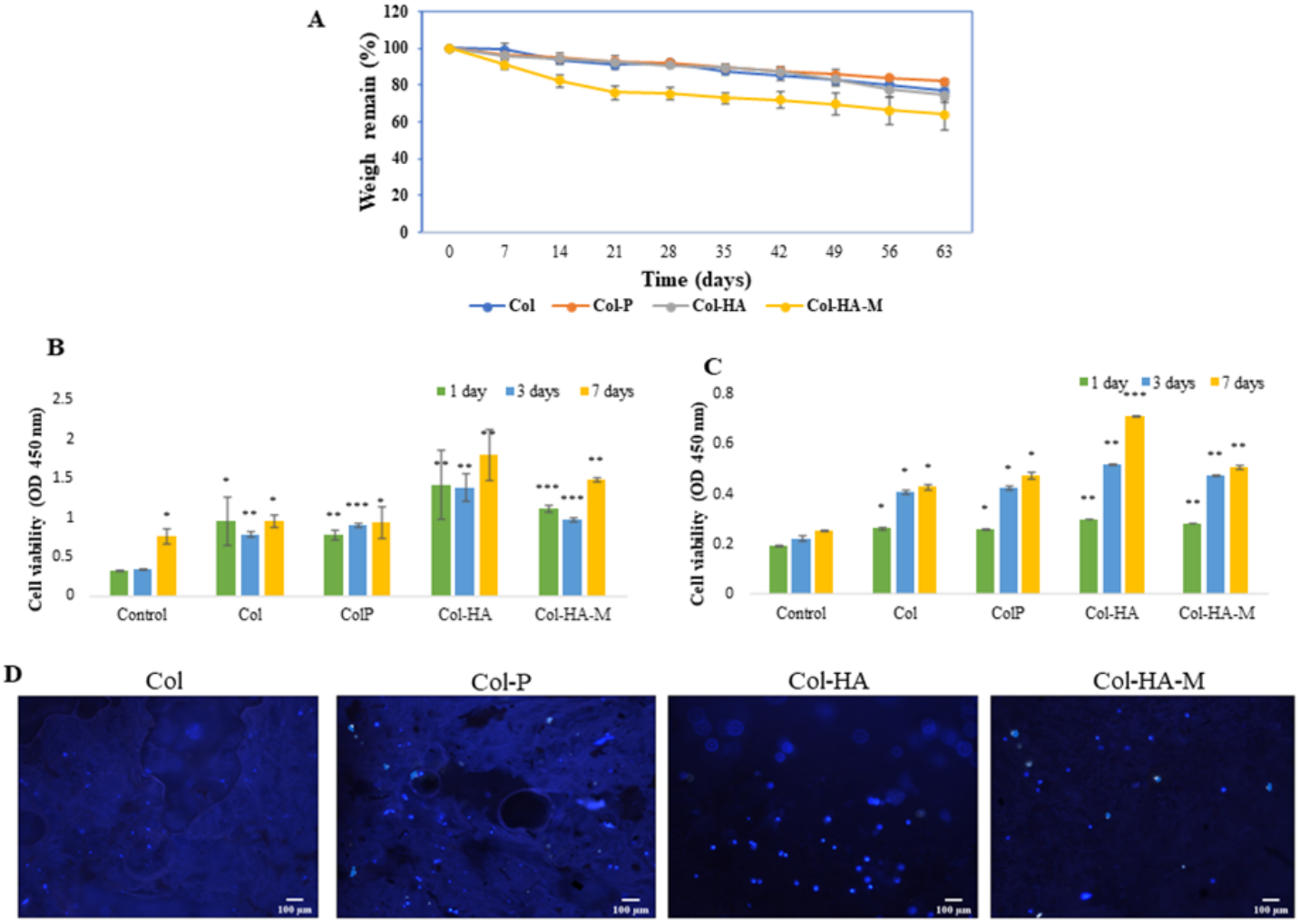

Figure 6

(A) The degradation rate of 3D scaffolds and 2D membrane as a function of time (n=3).(B) Cell viability of rBMSCs and (C) hADSCs on the Col, Col-P, and Col-HA scaffolds and Col-HA-M membrane. (D) DAPI staining after seeding hADSCs with materials for 7 days (10X), the light blue dots mean nucleic (n = 5, * $p < 0.05$, ** $p < 0.01$, *** $p < 0.001$).

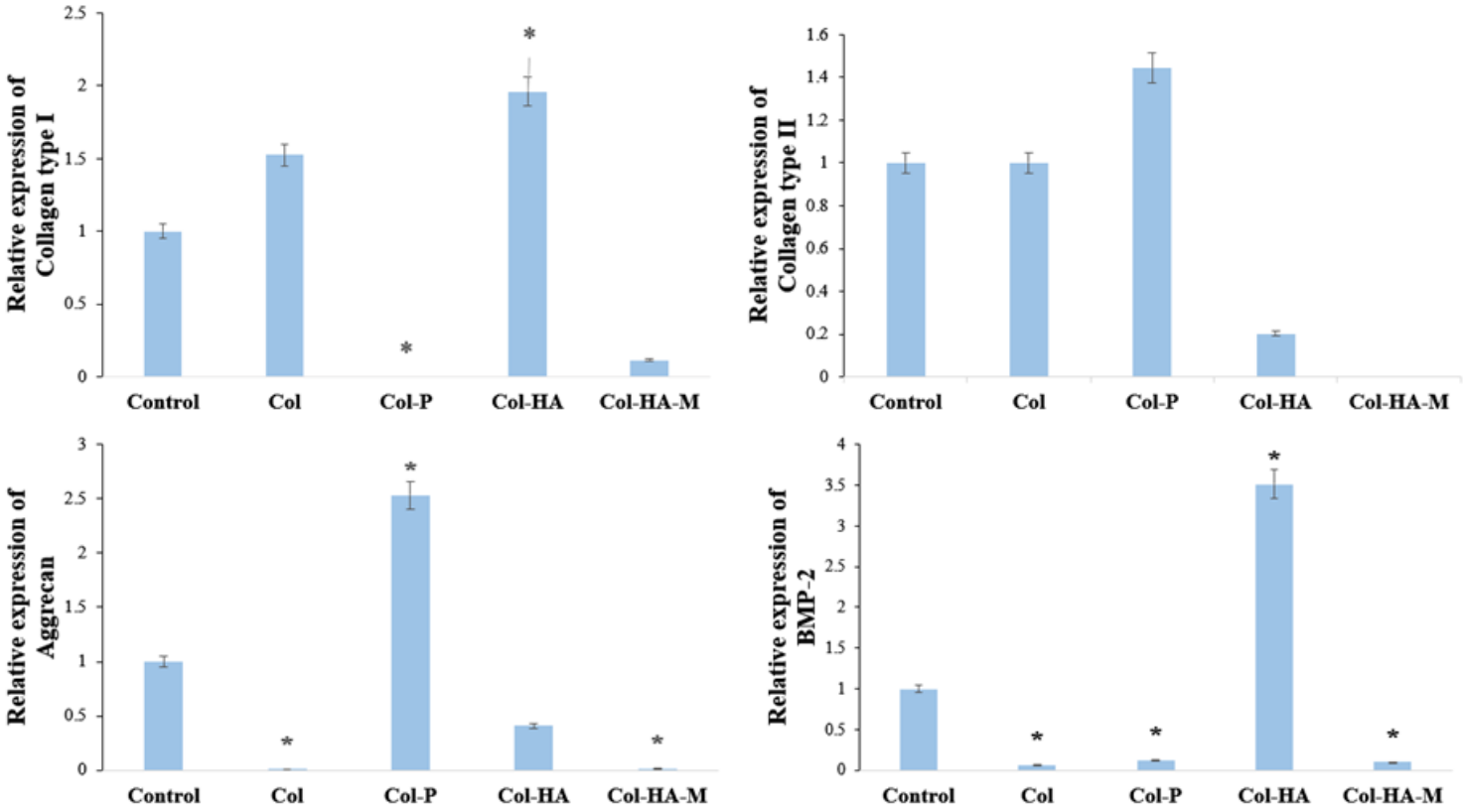

Figure 7

Gene expression for the differentiation of rBMSCs such as Col I, Col II, Aggrecan, and BMP-2 seeded on the scaffolds and membrane for 14 days. The genes of interest compare to the control-GAPDH (n=3, * $p<0.05$).

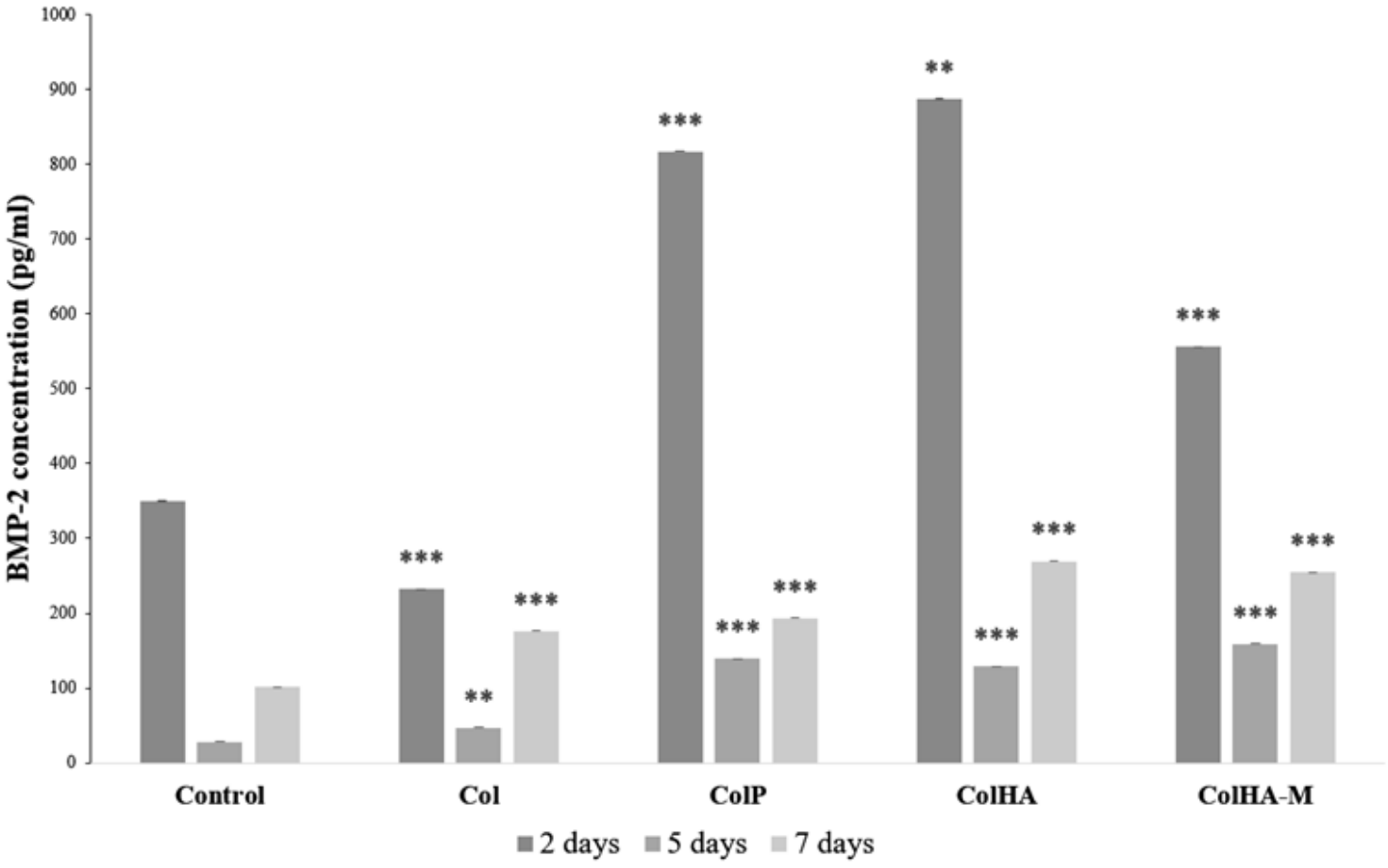

Figure 8

BMP-2 concentration of hADSCs culture on the 3D scaffolds and 2D membrane for 2, 5, and 7 days

(n = 3, * $p < 0.05$, ** $p < 0.01$, *** $p < 0.001$).

Figure 9

H&E staining of the collagen-based 3D scaffolds and 2D membrane implanted in the nude mice model after weeks 1, 2, and 4.

Figure 10

H&E staining of the collagen-based 3D scaffolds and 2D membrane implanted in the rat model after weeks 1, 2, and 4.